CHAPTER V

RESULTS AND DISCUSSION

5.1 Structural properties of BTO and Fe-doped BTO thin films

In this section, first we will briefly explain the X-ray diffraction result of BTO and Fe-doped BTO thin films, then the surface morphology of the BTO film with 6 layer compare with Fe-doped BTO thin films with 8 layer. Finally, the composition of Fe-doped BTO thin films will be presented.

5.1.1 X-ray diffraction pattern of BTO and Fe-doped BTO thin films

4.3 UV-VIS-NIR preparation

A Perkin-Elmer Lambda 750 UV-Vis-NIR spectrophotometer was used to determine transmission spectra of the film. The samples (quartz substrates and the thin films) are held with a box acelic. Quartz substrate as a reference was put at R position (shown in Fig. 3.6) and the thin film was put at S position (shown in Fig. 3.6). The wavelength used in the experiment was in the range of 300 nm to 1200 nm with the increment 0.1 nm. The light source is on the left side and the detector is on the right side of the Fig. 4.8, respectively. The results of optical properties of Fe-doped BTO and Fe-doped CCTO thin films before and after gamma ray irradiation will be shown in section 5.2 and 5.4, respectively.

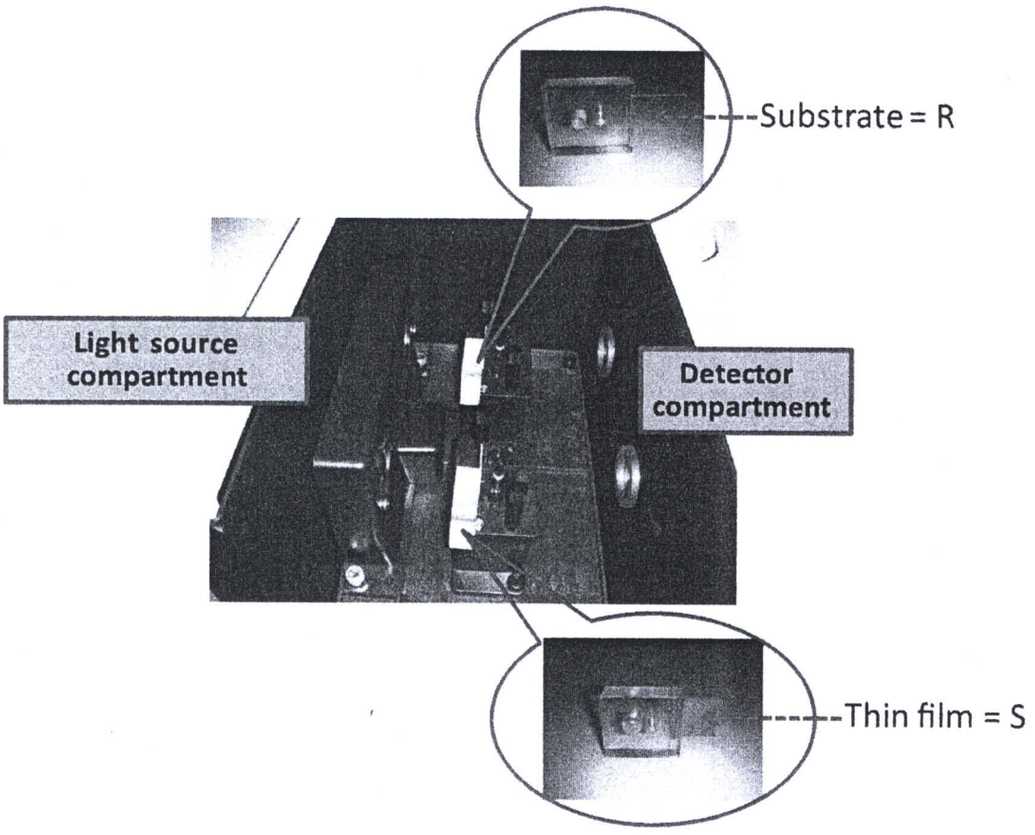

Figure 4.8: The set up process of UV-VIS-NIR spectrometer.

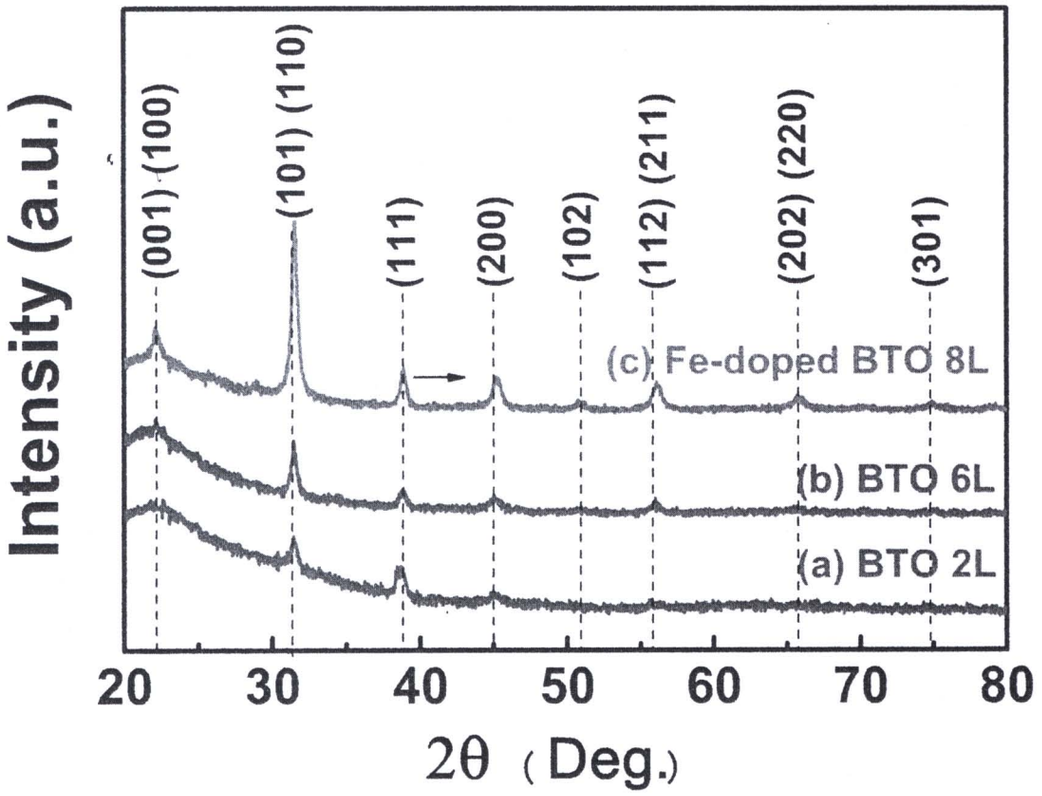

Figure 5.1: X-ray diffraction patterns of (a) BTO film with 2 layers (b) BTO film with 6 layers (c) Fe-doped BTO film with 8 layers.

The X-ray diffraction patterns of BTO and Fe-doped BTO films were recorded to determine their crystal structures. Figure 5.1 shows the XRD patterns of BTO with 2 and 6 layers as well as that for Fe-doped BTO films with 8 layers, derived from a sol-gel method. We denoted each film by the material formula followed by the number of layers (L). The tetragonal phase of BTO was identified in our films and it is indicated in Fig. 5.1 by the peaks with the indices of its crystallographic planes. The diffraction peaks are sharper and more intense as the films grow thicker through the deposition of more layers. The peak positions slightly shifted to higher diffraction angles after doping Fe in the film indicating that the lattice constants slightly decreased. From equation 3.2, the peak position for (200) and (101) was used to calculated the lattice constant (a-axis and c-axis)of BTO and Fe-doped BTO. The lattice constants of BTO with 6L are 4.005 Å and 4.021 Å for a-axis and c-axis. The lattice constants of Fe-doped BTO with 8L are 3.994 Å and 4.033 Å, respectively. This could be attributed to the substitution of ions with smaller size Fe^{3+} (0.64 Å) to ions with bigger size Ba^{2+} (1.34 Å). These results are consistent with the work of other groups [4, 46]. Figure 5.2 shows X-Ray diffraction patterns of (a) $BaTiO_3$ film before and after gamma ray dose of 1 kGy (b) Fe-doped BTO film before and after gamma ray dose of 1 kGy, respectively. The XRD pattern of both films did not change after gamma irradiation dose of 1 kGy. In Fig. 5.2, the diffraction peaks are sharper and more intense and the peak position slightly shifted to higher diffraction angles (see in Fig. 5.3) after BTO doped with Fe.

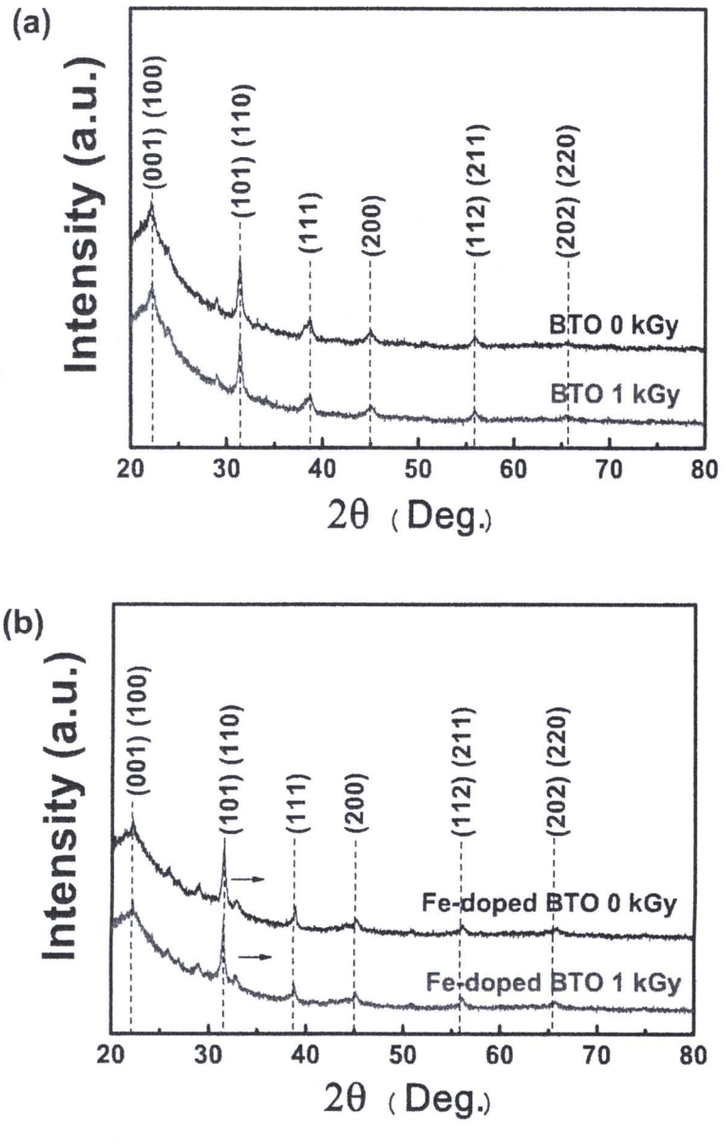

Figure 5.2: X-ray diffraction patterns of (a) BTO film before and after gamma ray dose of 1 kGy (b) Fe-doped BTO film before and after gamma ray dose of 1 kGy.

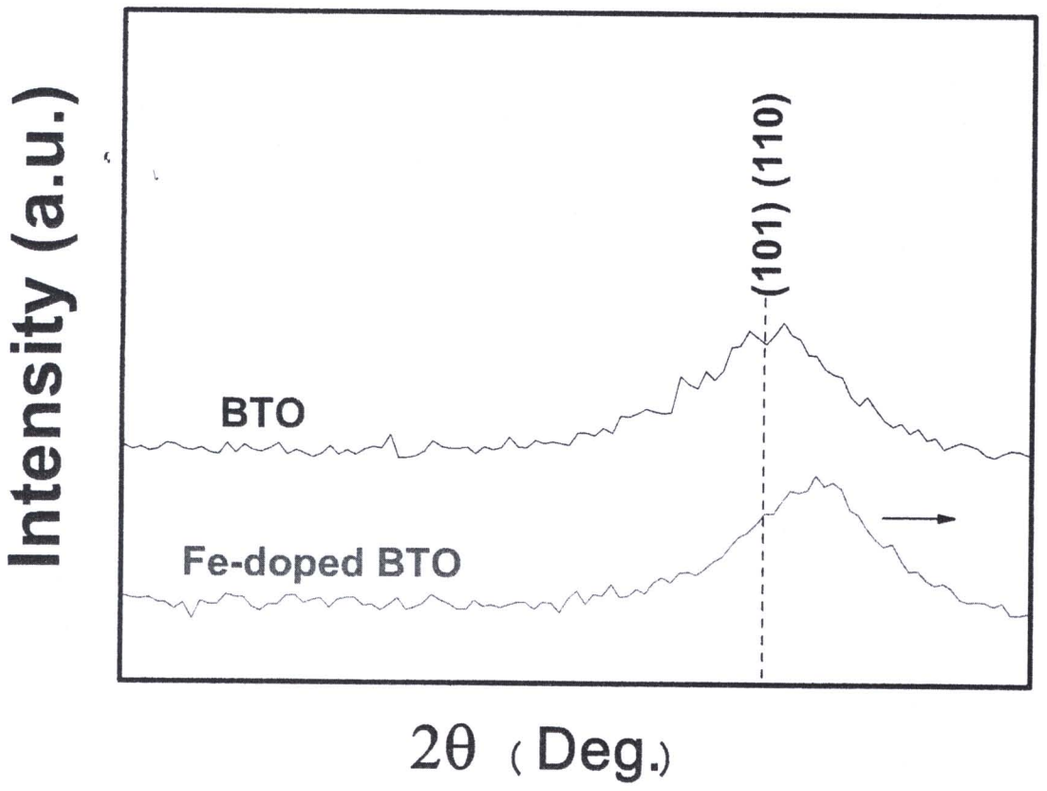

Figure 5.3: X-ray diffraction patterns of BTO and Fe-doped BTO film before and after gamma ray dose of 1 kGy zoom at (101), (110).

5.1.2 Surface morphology of BTO and Fe-doped BTO thin films

The surface morphology of the BTO and Fe-doped BTO films was observed using a Veeco Nanoscope IV atomic force microscope (AFM). The estimated average grain size of the Fe-doped BTO 8L film is 40 nm which is smaller than the 54 nm grain size for the 6L film as seen in Fig. 5.4. Devan et al. observed similar results with a decrease in grain size with doping concentrations [46]. Indeed, many research groups have reported that increasing the dopant concentration could reduce the grain size due to competition between different phase structures in the materials [2, 4].

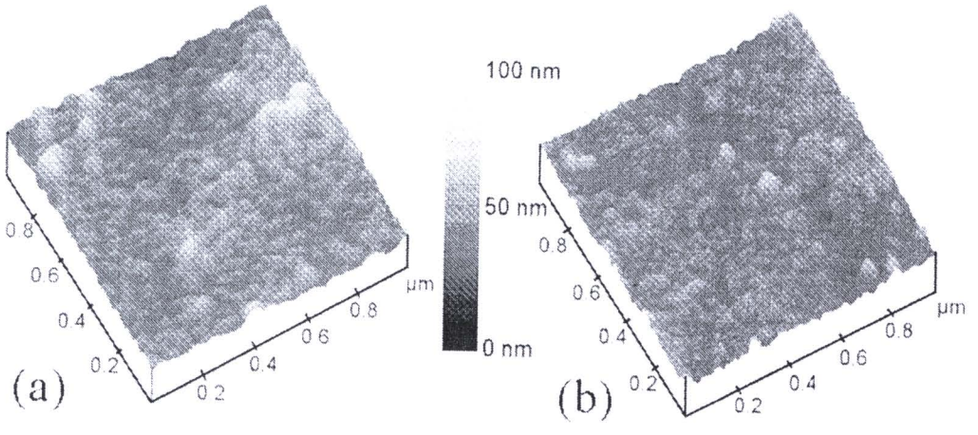

Figure 5.4: Atomic force microscopy images (1.0 × 1.0 μm) of the films comprised of (a) BTO with 6L (b) Fe-doped BTO with 8L.

5.1.3 Composition of Fe-doped BTO thin films

The compositions of the films were obtained using a WDX equipped with an electron probe microscopic spectrometer (EPMS: JEOL model JXA-8100). In the beginning, we have planned to dope Fe with 10% by weight for BTO. However, the quantity of Fe in our films was not the same as the calculation, and later is confirmed from WDX experiment. The obtained concentration of Fe is 7% by weight instead of 10% by weight. The substitution site for the dopant cation depends more strongly on its concentration and on the Ba/Ti molar ratio than on its size. The ionic radius of Fe^{3+} (0.64 Å) is comparable with the ionic radius of Ti^{4+} (0.68 Å) but is significantly different from that for Ba^{2+} (1.34 Å) [4]. However, the WDX shows signals that are consistent with $Ba_{0.8}Fe_{0.2}TiO_3$ as shown in Table 5.1 with the Fe doping occurring by substitution of Ba sites in BTO yielding a Ba/Ti ratio slightly smaller than 1. The oxidation state determined from the energy of the X-ray absorption edge (7130.5 eV) corresponds to Fe^{3+}. The X-ray absorption experiment was done by Thidarat Supasai, a Ph.D student at Department of physics, Chulalongkorn University. In our case the Fe^{3+} dopant acts as a donor when it substitutes the Ba^{2+} site that means our doped BTO films are n-type semiconductor. A similar result for this substitution was found in the work of Battisha et al. [1].

Table 5.1: Mass (%), Atom (%) and Ratio of Fe-doped BTO.

	Mass (%)	Atom (%)	Ratio
Ba	66.293	41.159	0.8
Fe	4.552	6.9471	0.2
Ti	29.154	51.8939	1
	100	100	

5.2 Optical properties of BTO and Fe-doped BTO thin film

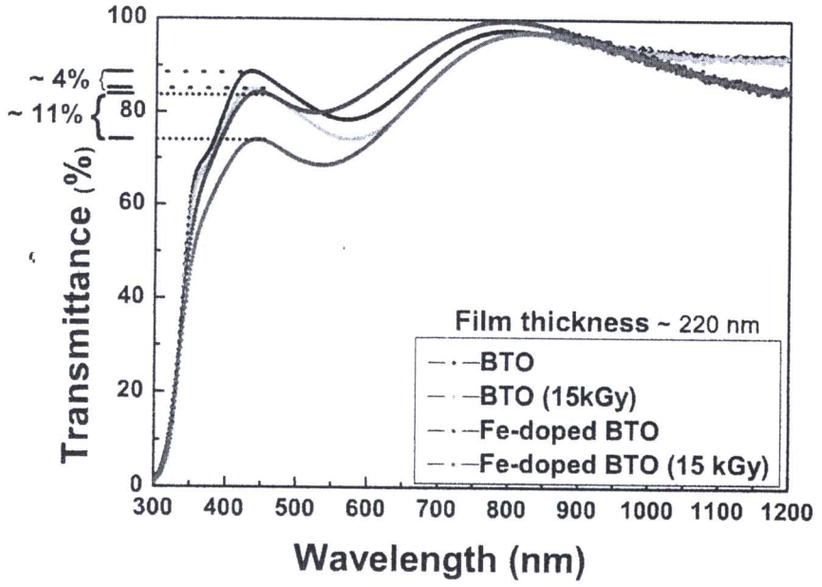

Figure 5.5: The transmission spectra of BTO and Fe-doped BTO thin films before and after gamma irradiation at a dose of 15 kGy.

The optical transmittance spectra of the films using a Perkin-Elmer Lambda 750 UV-Vis-NIR spectrophotometer were measured after gamma irradiation immediately. Figure 5.5 shows the optical transmission spectra in the 300 - 1200 nm wavelength range of the BTO and Fe-doped BTO films of comparable thickness (ca. 220 nm) before and after gamma irradiation at 15 kGy. The oscillation in the transmission curve is due to interference between light reflecting from the film surface and from the film-substrate interface. The depth of modulation indicates good homogeneity of the films across the light beam (ca. 1 cm in diameter). The transmittance of both BTO and Fe-doped BTO films were reduced after the irradiation, and a brownish tint could be seen by the naked eye in the irradiated films (Fig. 5.6). It is believed that structural defects after gamma irradiation causes a

change in the color of films as well as the change in color observed in jewelry. This phenomena is called color center. From the Section 2.4, the color center occurs when the gamma ray kicks out Ba or Ti or O atoms leaving atom vacancies. The atom vacancy are often occur at O site rather than Ba or Ti sites in $BaTiO_3$.

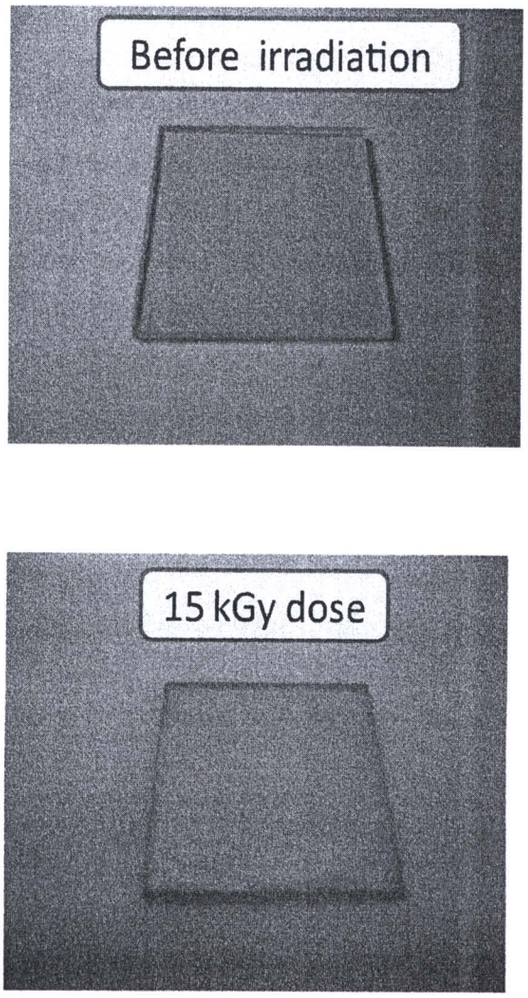

Figure 5.6: Fe-doped BTO thin films before and after gamma irradiation at a dose of 15 kGy.

However, our results revealed that gamma irradiation causes a more marked change on the transmittance of the Fe-doped BTO film than to the BTO film. For comparison, following gamma irradiation at 15 kGy, the transmittance decreased by 4% in the BTO film but by 11% for the Fe-doped BTO film. It seems that the trapping process in the films after irradiation occurs more readily in the doped films, presumably because they have more defects than in BTO films.

Fig. 5.7(a) shows the optical transmission spectra of Fe-doped BTO films with 4L and 6L (denoted by Fe-doped BTO 4L and Fe-doped BTO 6L, respectively) in the 300 - 1200 nm wavelength range and Fig. 5.7(b) shows the same trend for the Fe-doped BTO film with 8L (denoted by Fe-doped BTO 8L). As expected, the thicker film shows deeper oscillations in the transmission spectrum than the thinner film. The transmittance also decreased with the increasing gamma radiation doses. The doses used in this study were 1, 5, 10 and 15 kGy, respectively. We observed that the transmittance of the films did not change any further for gamma radiation doses higher than ca. 10 kGy. The absorption edge shifted to a lower energy as the films got thicker (Fig. 5.7(a)), because the films with a larger number of layers accumulated longer heating times (800 ^{0}C for 60 min for each layer) causing the growth of bigger grains. However, there was little variation in the absorption edge between the Fe-doped BTO 4L film annealed for four hours and Fe-doped BTO 8L film annealed for eight hours. The film thickness of Fe-doped BTO ranging from four to eight layers were calculated via the envelope method derived by Swanepoel [47] and were approximately 220 nm (4L), 375 nm (6L) and 520 nm (8L).

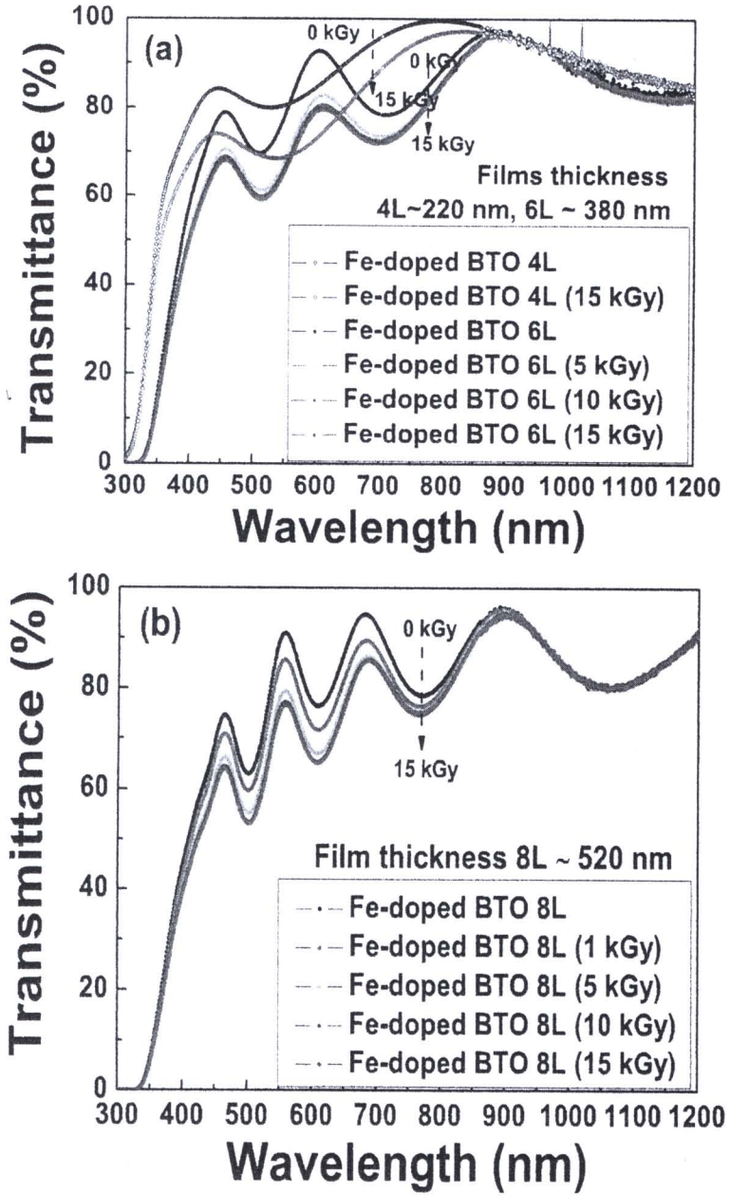

Figure 5.7: The transmission spectra of (a) Fe-doped BTO films with 4L, 6L and (b) Fe-doped BTO films with 8L, after exposure to different gamma radiation doses.

From the transmittance spectra, the energy for the direct gap could be calculated by using the Equation 3.11: $(\alpha h\nu)^2 = B(h\nu - E_g)$ where α is the absorption coefficient, $h\nu$ is the photon energy, E_g is the energy gap and B is a constant.

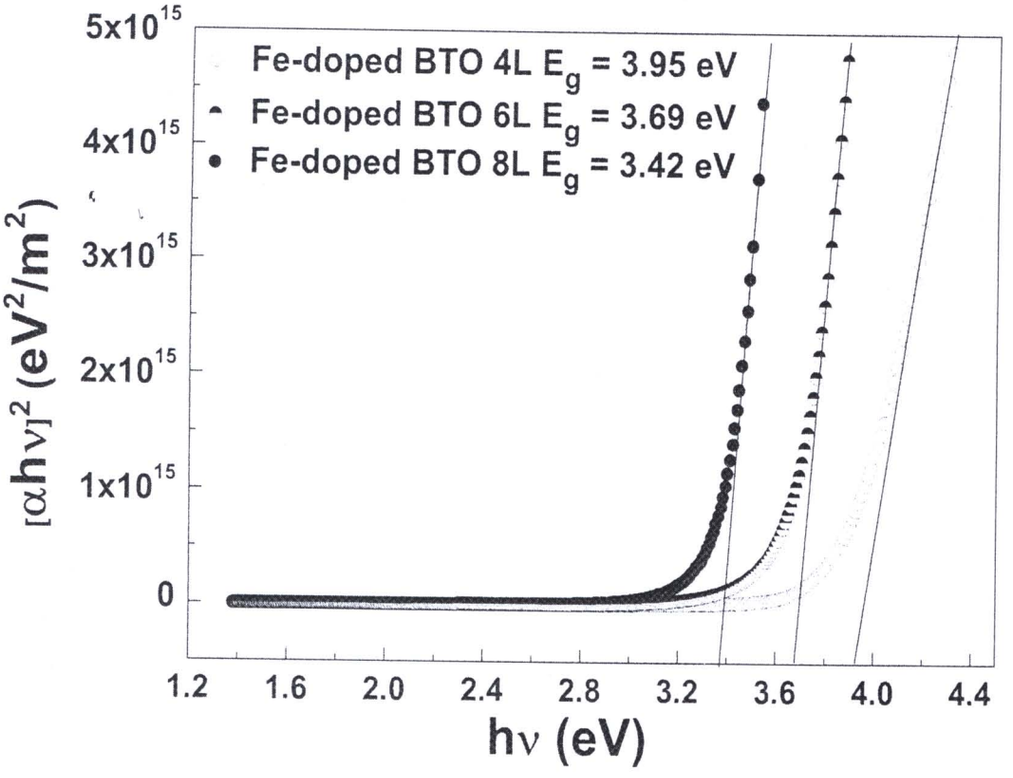

Figure 5.8: Plot between $(\alpha h\nu)^2$ versus $h\nu$ of Fe-doped BTO thin films with 4L 6L and 8L, respectively.

The energy band gap of Fe-doped BTO with 4L, 6L and 8L did not change after gamma exposure to different gamma radiation doses as shown in Fig. 5.9.

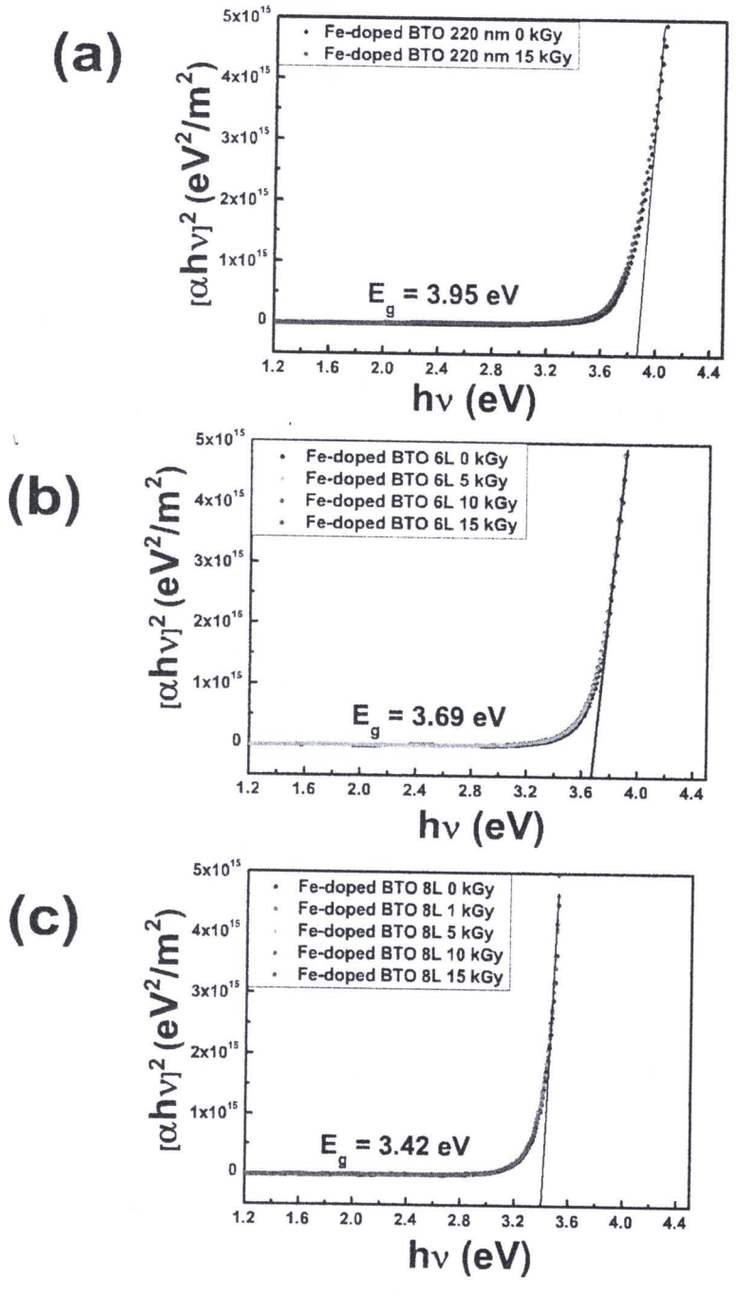

Figure 5.9: Plot between $(\alpha h\nu)^2$ versus $h\nu$ of Fe-doped BTO thin films before and after exposure to different gamma radiation doses (a) 4L (b) 6L and (c) 8L, respectively.

Figure 5.10, 5.11 and 5.12 show the plot between $\ln\alpha$ versus $h\nu$ of Fe-doped BTO with 4L, 6L and 8L, respectively. The measurement of the band edge characteristic can be obtained from the so called Urbach rule. In general, an exponentially increasing absorption edge can be seen in various types of materials;

$$\alpha = \alpha_0 e^{(\frac{\sigma(h\nu - E_0)}{kT})} = \alpha_0 e^{(\frac{h\nu - E_0}{E_u})} \tag{5.1}$$

where α_0 and E_0 are the Urbach bundle convergence point coordinates, E_u is the absorption edge energy width interpreted as the width of the tails of localized states in the band gap as shown in Fig. 3.9, Section 3.5.2 and σ is the steepness parameter, k is the Boltzmann constant and T is the temperature.

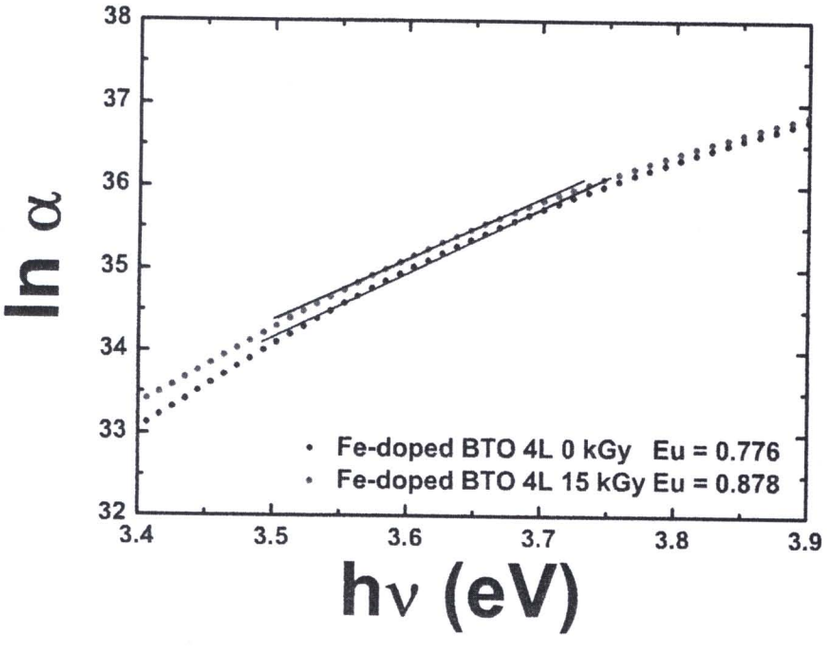

Figure 5.10: Determination of the Urbach energy for Fe-doped BTO 4L with gamma irradiation doses of 15 kGy.

As the gamma radiation dose increased, the absorption edge energy width of Fe-doped BTO with 4L increase from 0.776 to 0.878 eV after 15 kGy indicating that the gamma ray induced more defects.

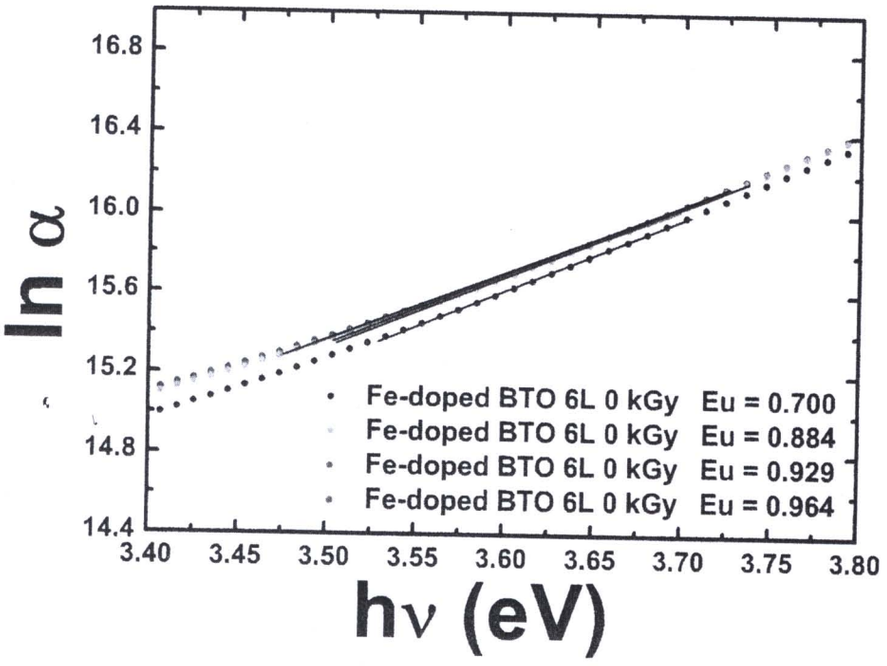

Figure 5.11: Determination of the Urbach energy for Fe-doped BTO 6L with different gamma irradiation doses.

In the similar way, the absorption edge energy width increases with the gamma radiation dose. The absorption edge energy width of Fe-doped BTO with 6L increase from 0.700 to 0.964 eV after 15 kGy indicating that the gamma ray induced more defects.

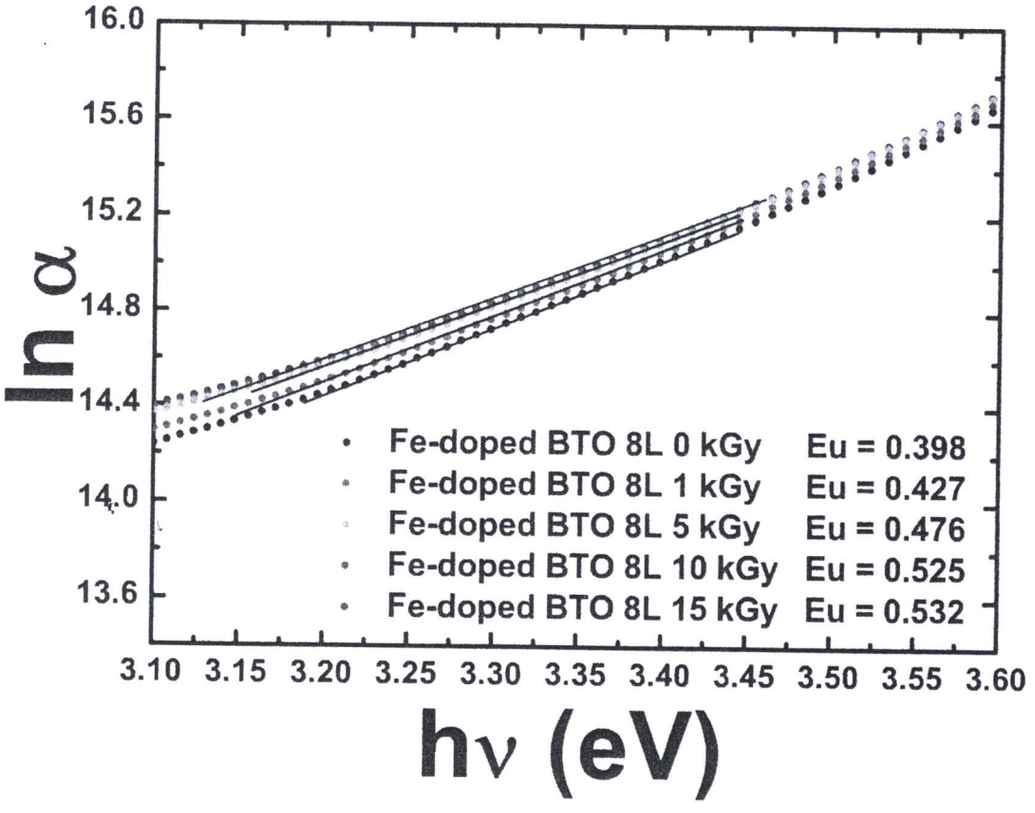

Figure 5.12: Determination of the Urbach energy for Fe-doped BTO 8L with different gamma irradiation doses.

The same trend can be seen in the data of Fe-doped BTO with 8L. The absorption edge energy width of Fe-doped BTO with 8L increase from 0.398 to 0.532 eV after 15 kGy.

Figure 5.8 shows a plot between $(\alpha h\nu)^2$ versus $h\nu$ of the Fe-doped BTO thin films with 4, 6 and 8 layers. The resulting energy band gaps were 3.42 eV, 3.69 eV and 3.95 eV for Fe-doped BTO with 8, 6 and 4 layers, respectively. For comparison, the energy band gap value of pure BTO powder, BTO single crystal, and BTO thin films are 3.92 eV [48], 3.6 eV [49] and 3.72-3.77 eV [50], respectively. The particle size in these films increases as the annealing cycle increases [51]. The corresponding reduction in band gap energy with increasing particle size can be explained by quantum confinement [37, 52]. By way of comparison, we used the quantum confinement prediction for energy gap.

$$E_g(r) = E_g(bulk) + \frac{2\pi^2 h^2}{r^2}\left(\frac{1}{|m_e|} + \frac{1}{|m_h|}\right) \tag{5.2}$$

$$E_g(r) = E_g(bulk) + \frac{2\pi^2 h^2}{r^2 \mu} \tag{5.3}$$

where m_e, m_h, μ and r are the effective mass of electron, the effective mass of hole, the reduced mass and the diameter of nanoparticle, respectively. Normally, if the particle size is smaller than the corresponding DeBroglie wavelength, the size quantization effects can be observed in the band gap. The theoretical calculated DeBroglie wavelength for BTO is about 15 nm.

$$a_B = (4\pi\varepsilon_0\varepsilon_r\hbar^2)/\mu e^2$$

Analysis of the variation of the dispersion curves of Fe-doped BTO films after different gamma irradiation doses (0-15 kGy) reveal that the refractive index and the extinction coefficient increase with the wavelength rising more rapidly toward short wavelengths and following a typical dispersion curve shape (Fig. 5.13). When measured in the 350 - 750 nm wavelength range, the refractive index (n) for the Fe-doped BTO 4L increased from 2.17 - 1.88 range to 2.34 - 1.95 range upon the gamma irradiation at a dose of 15 kGy, with a corresponding increase in the extinction coefficient (k) (Fig. 5.13(a) and (b)). The value of the extinction

coefficient for this film prior to gamma irradiation was in the order of 10^{-2} and this increase after the irradiation with higher doses, indicating that higher optical losses result directly from the irradiation. With thicker films, the refractive index is also increased due to the increased film density and better crystallinity as shown in Fig. 5.14. While the extinction coefficient of BTO 4L, 6L and 8L films did not change much. The extinction coefficient follows an approximately linear function of the wavelength. The dispersion curves near the electronic band transition were significantly altered by the gamma irradiation. One of the main results of these experiments is that the complex refractive index of the films can be tuned by exposure to various gamma rays doses. These observed phenomena could be useful for the development of gamma irradiation dosimeters based on simple optical detection properties.

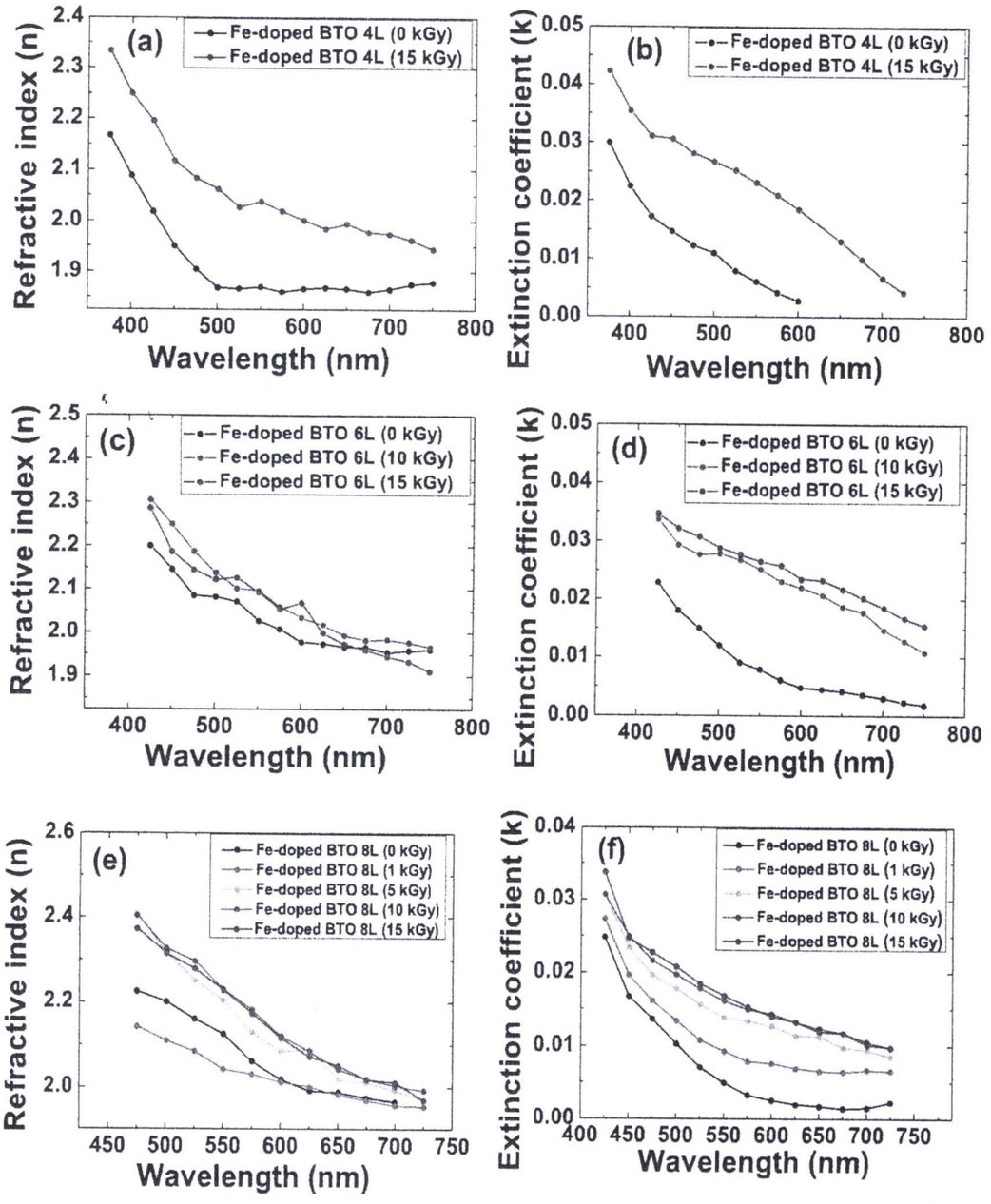

Figure 5.13: (a,c,e) The refractive index of Fe-doped BTO thin films with 4L 6L and 8L, respectively and (b,d,f) the extinction coefficient of Fe-doped BTO thin films with 4L 6L and 8L, respectively.

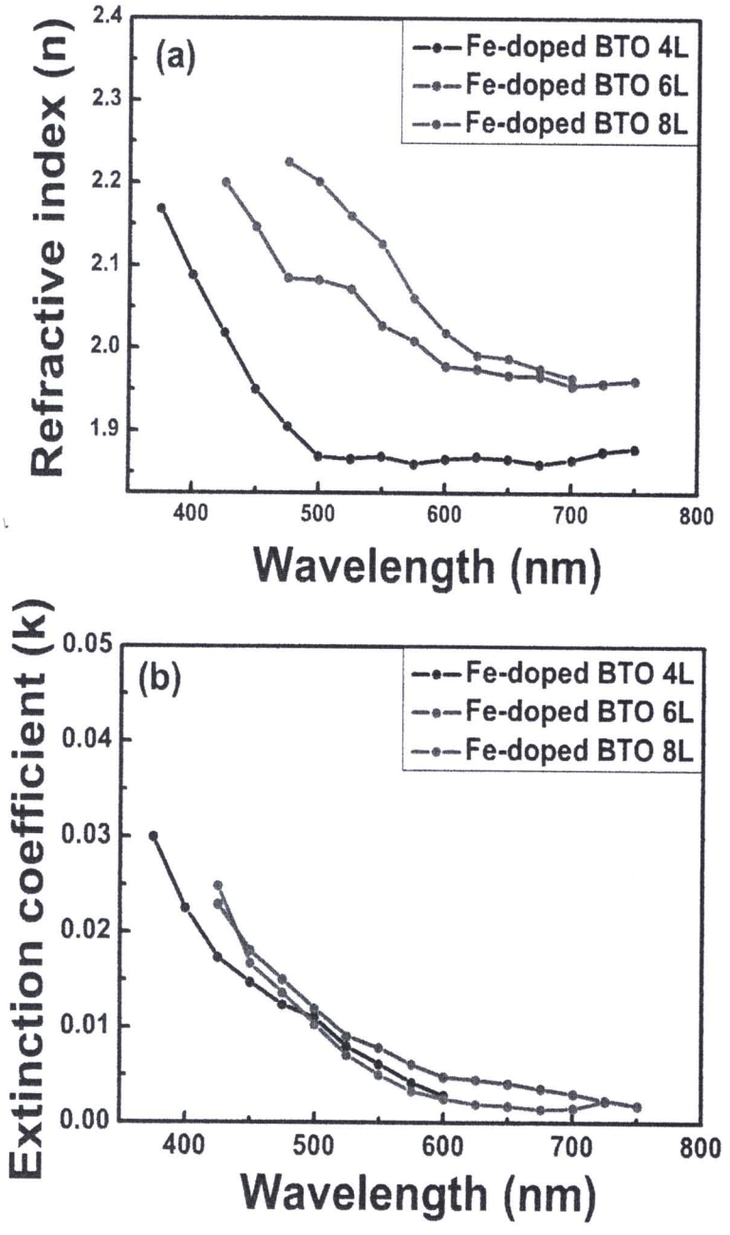

Figure 5.14: The refractive index of Fe-doped BTO thin films with 4L 6L and 8L, respectively.

5.3 Structural properties of CCTO and Fe-doped CCTO thin films

In this section, the XRD patterns of CCTO and Fe-doped CCTO thin films were used to confirm the crystalline of the film and EDX used to confirm the composition for Fe in the Fe-doped CCTO films.

5.3.1 X-ray diffraction pattern of CCTO and Fe-doped CCTO thin films

The X-ray diffraction patterns of CCTO and Fe-doped CCTO thin films were recorded to determine their crystal structures. Figure 5.15 shows the XRD patterns of CCTO and Fe-doped CCTO films. From equation 3.3, peak (220) was used to calculate the lattice constants of the films. The lattice constant of CCTO is 7.3877 Å while Fe-doped CCTO with lattice constant is 7.3799 Å, respectively. In Fig. 5.15, the peak positions of CCTO film slightly change after doping Fe in the film indicating that Fe substituting for Cu (see Section 5.3.2) and Fig. 5.16 shows X-ray diffraction pattern of Fe-doped CCTO thin films before and after gamma ray dose of 1 kGy. The XRD pattern of Fe-doped CCTO films did not change after gamma irradiation dose of 1 kGy.

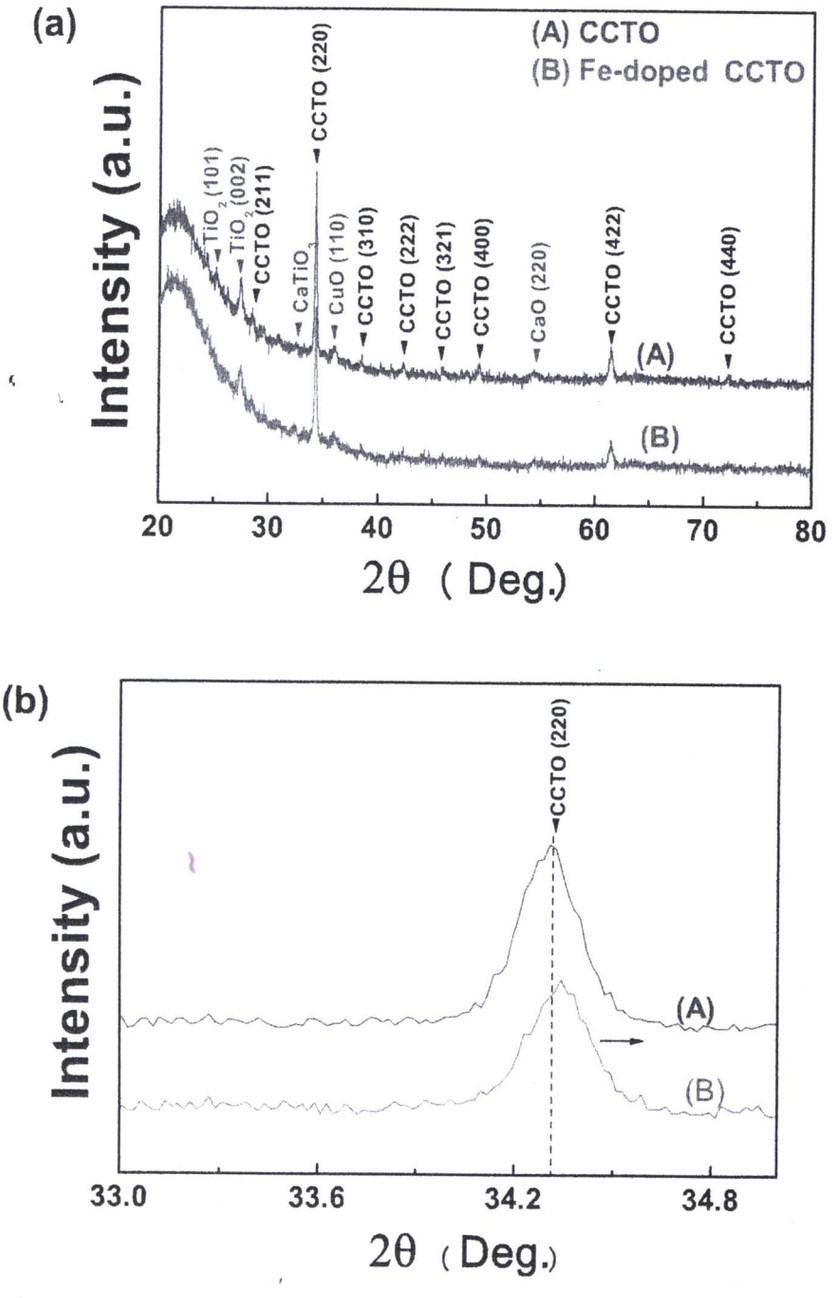

Figure 5.15: X-ray diffraction patterns of CCTO and Fe-doped CCTO thin films.

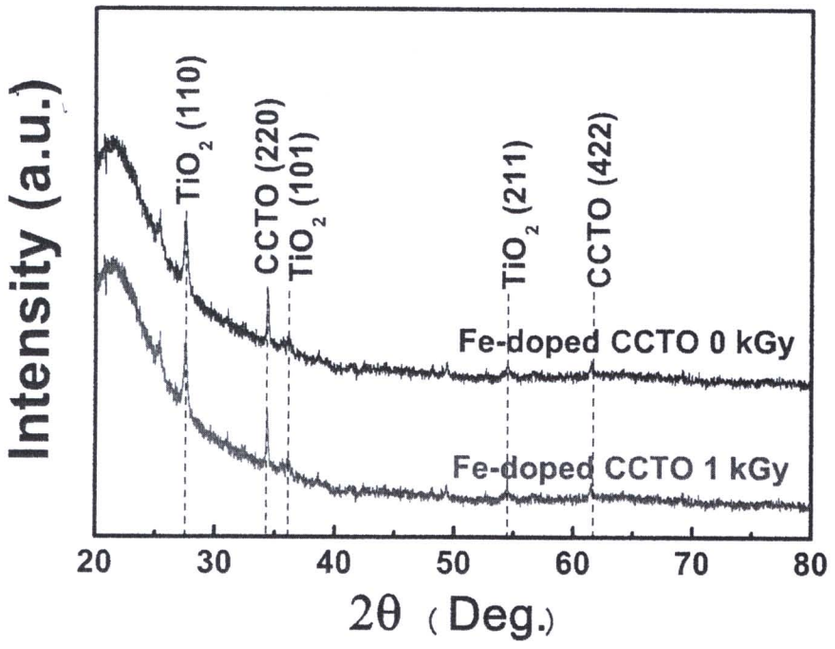

Figure 5.16: X-ray diffraction patterns of Fe-doped CCTO thin films before and after gamma ray dose of 1 kGy.

5.3.2 Energy dispersive X-ray data of Fe-doped CCTO

The compositions of the films were obtained using a EDX equipped with Field Emission Scanning Electron Microscopy (FSEM: HITASHI model S-4700). Table 5.2 shows the ratio of intensity and weight (%) of each atom in CCTO. The concentration of Fe doped 2% by weight for CCTO were choosed in this thesis. EDX experiment shown that Fe concentration of CCTO is 2.44%. Table 5.2 shows the intensity, weight (%) and rtatio of each atom in CCTO. The ratio of Ca:Cu:Ti:O is 1:1.5:5.2:10.3 indicating the excess Ti and the insucient Cu and O constitutions. The excess of Ti obtained from EDX consistent with the TiO_2 phase formation in XRD result. Table 5.3 shows the intensity, weight (%) and ratio of each atom in Fe-doped CCTO. The ratio of Ca:Cu:Fe:Ti:O is 1:1.5:0.4:3.6:8.6 indicating that Fe atoms are present in the film by substitution of Cu sites in the CCTO film. However, from this result we found that the amount of Cu was insufficient in the film.

Table 5.2: Intensity, Weight (%) and Ratio of CCTO.

	Intensity (c/s)	Weight (%)	Ratio
Ca	61.72	8.273	1
Cu	2.44	20.264	1.5
Ti	172.47	39.555	5.2
O	100.56	27.575	10.3
		100	

Table 5.3: Intensity. Weight (%) and Ratio of Fe-doped CCTO.

	Intensity (c/s)	Weight (%)	Ratio
Ca	57.57	8.215	1
Cu	1.73	15.419	1.5
Fe	6.52	5.782	0.4
Ti	169.55	41.644	3.6
O	96.12	28.939	8.6
		100	

5.4 Optical properties of Fe-doped CCTO

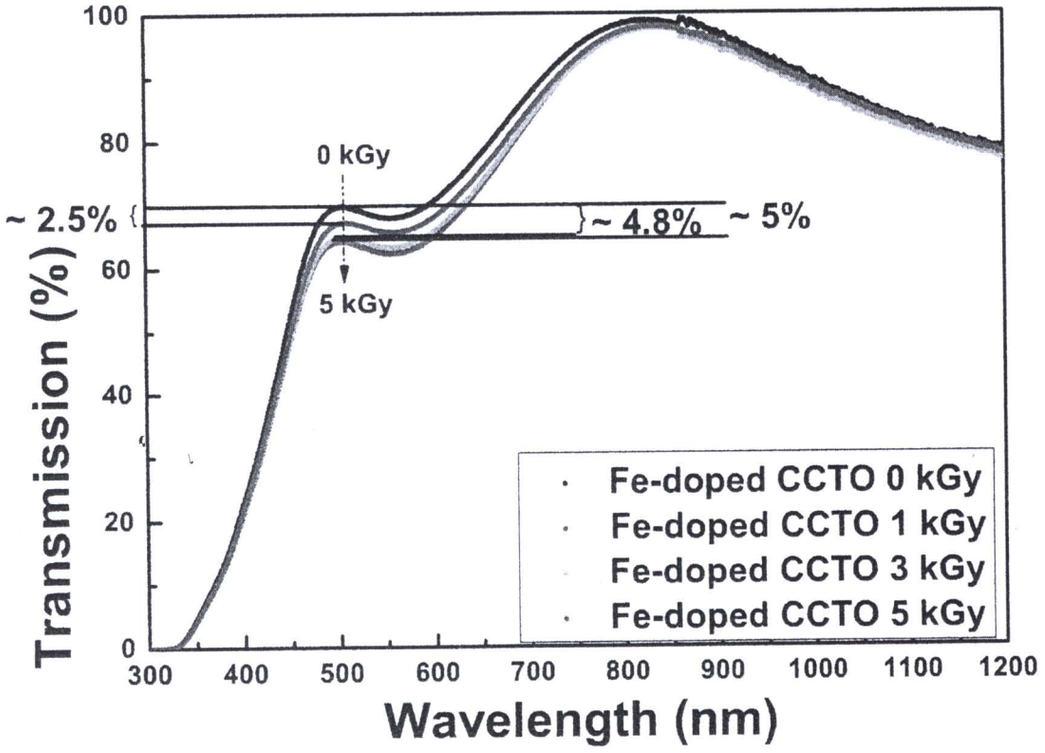

Figure 5.17: The transmission spectra of Fe-doped CCTO thin films for different gamma radiation dose.

Figure 5.17 shows the optical transmission spectra in the 300-1200 nm wavelength range of Fe-doped CCTO films before and after gamma irradiation at 1, 3 and 5 kGy dose, respectively. The depth of modulation normally indicates that the films are homogeneous.

We have found the reduction in transmittance decreasing to 2.5%, 4.8% and 5.0% after exposure with gamma irradiation dose of 1 kGy, 3 kGy and 5 kGy, respectively. We observed that the transmittance of the films did not change after the gamma radiation dose is higher than ca. 3 kGy. In another word, there was not much change in the transmittance for the film exposed with 3 kGy and 5 kGy. This could be due to the saturation of activity of color centers phenomena. There were not much change in the percentage transmission of Fe-doped CCTO film as

compared with BTO and Fe-doped BTO film. For example, BTO and Fe-doped BTO with thickness 220 nm decrease 4% and 11% after gamma irradiation with 15 kGy, while CCTO films with thickness of 360 nm decrease 5%, after irradiation with 5 kGy dose, respectively.

After gamma ray irradiation, the films became brownish tint. This color changes can be seen by naked eye (see in Fig. 5.18) but with less change in color compared to that of BTO and Fe-doped BTO films.

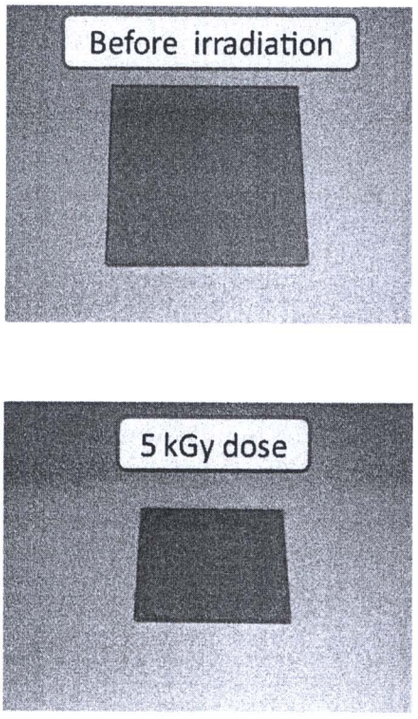

Figure 5.18: Fe-doped CCTO thin films before and after gamma irradiation at a dose of 5 kGy.

5.4.1 Energy gap

From the transmittance spectra in Fig. 5.17, the energy gap for direct gap could be calculated by using the equation 3.11. Figure 5.19 shows plot between$(\alpha h\nu)^2$ versus $h\nu$ of Fe-doped CCTO thin films. The resulting energy band gaps were 3.67 eV. The discrepancy will be further investigated. The refractive index can be obtained using envelope method from equation 3.9. The extinction coefficient can be obtained from equation 3.10. However, we focused on absorption region to extract some information as shown in Fig. 5.20

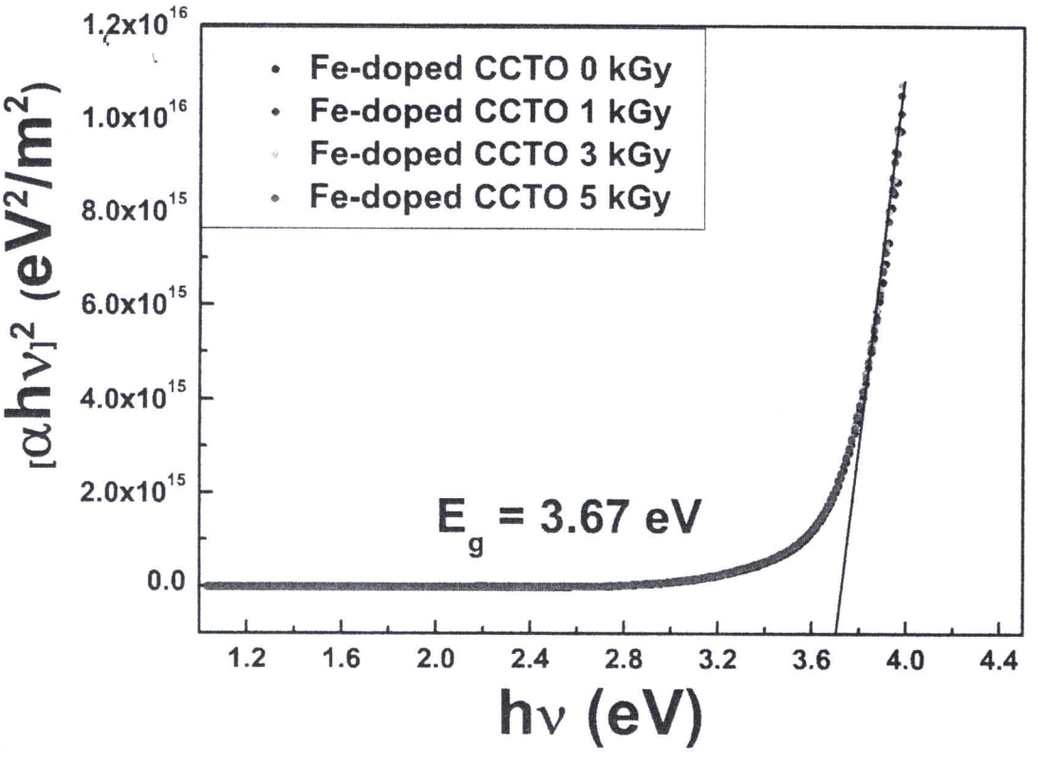

Figure 5.19: Plot between $(\alpha h\nu)^2$ versus $h\nu$ of Fe-doped CCTO thin films.

Figure 5.20 show the plot between $\ln\alpha$ versus $h\nu$ of Fe-doped CCTO films. As the gamma radiation dose increased, the absorption edge energy width increased from 0.2298 to 0.2778 eV after 5 kGy indicating that the gamma ray induced more defects.

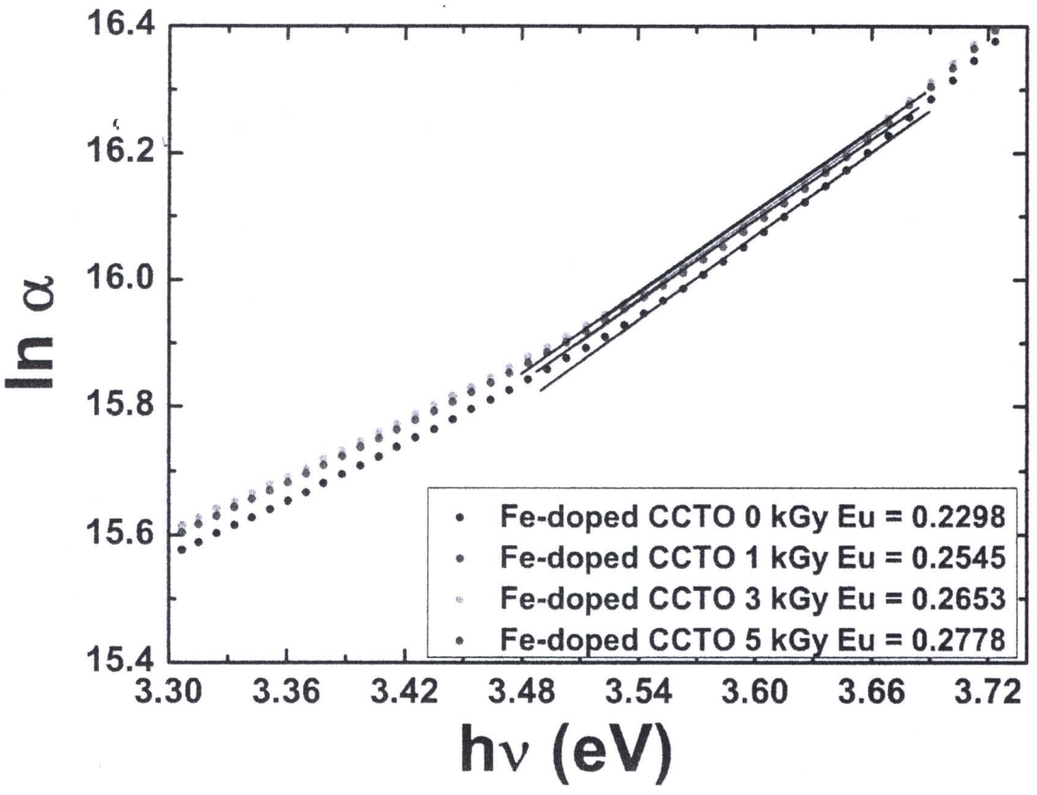

Figure 5.20: Determination of the Urbach energy for Fe-doped CCTO with difference gamma irradiation doses.

5.4.2 Complex refractive index (n and k) of Fe-doped CCTO

Figure 5.21 shows the refractive index and the extinction coefficient of the Fe-doped CCTO film measured in the 450-700 nm wavelength range. The refractive index of the films measured in this wavelength range increased from 2.24 - 2.00 range to 2.30 - 2.00 range for Fe-doped CCTO film upon the gamma irradiation with a 3 kGy dose with a corresponding increase in the extinction coefficient as shown in Figure 5.22. There was not much change in the refractive index of the films until the dose increased to 3 kGy. The increasing in the extinction coefficient with the irradiation dose indicates that high optical losses causing by the irradiation. The value of the extinction coefficient of the films before and after gamma irradiation was still on the order of 10^{-2}. The shape of refractive index was similar to the result of Raffaella et al.'s group [53].

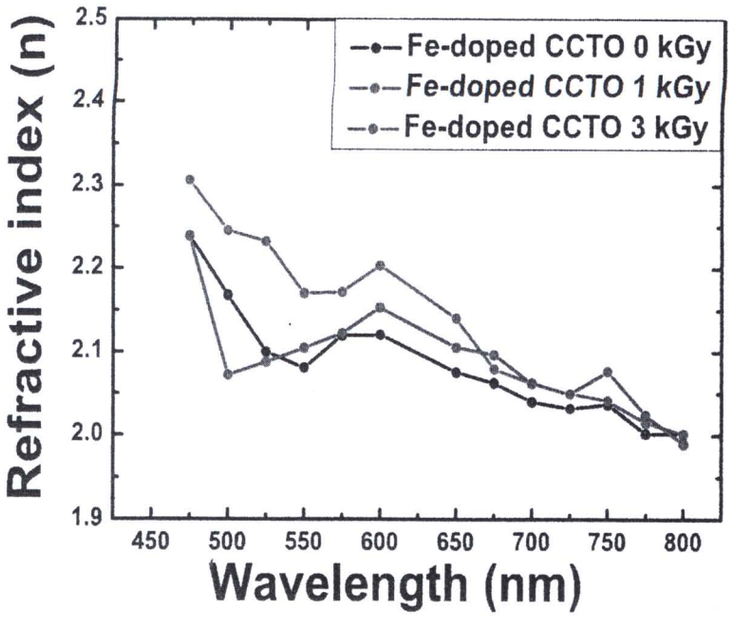

Figure 5.21: The refractive index of Fe-doped CCTO thin films for different gamma radiation dose.

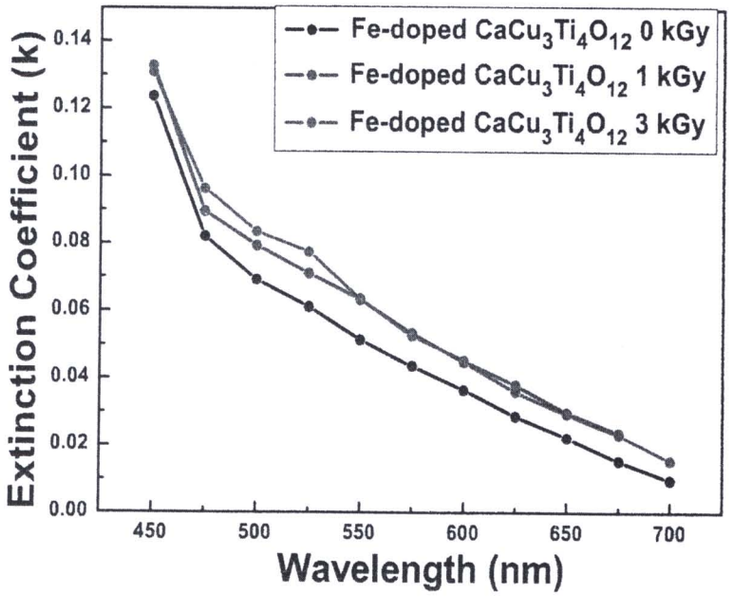

Figure 5.22: The extinction coefficient of Fe-doped CCTO thin films for different gamma radiation dose.

5.4.3 Capacitance of CCTO capacitor

CCTO film was grown on Al_2O_3 substrate which has insulator property. A HEWELETT PACKARD (HP): Model 4192A LCR IMPEDANCE ANALYZER was used to measure the capacitance of CCTO capacitor. When the electrodes are on the top of the film and on the same plane, the capacitor is so called a coplarnar capacitor. In general, the electrodes are in the form of interdigitate electrodes. The processing of interdigitated electrodes for this film can be read form Yamairoh Kasa's thesis [54]. Fig. 5.23 shows CCTO thin films with interdigitated electrodes. The gap width is 10μm and the overall size of capacitor is about 2×3 mm^2.

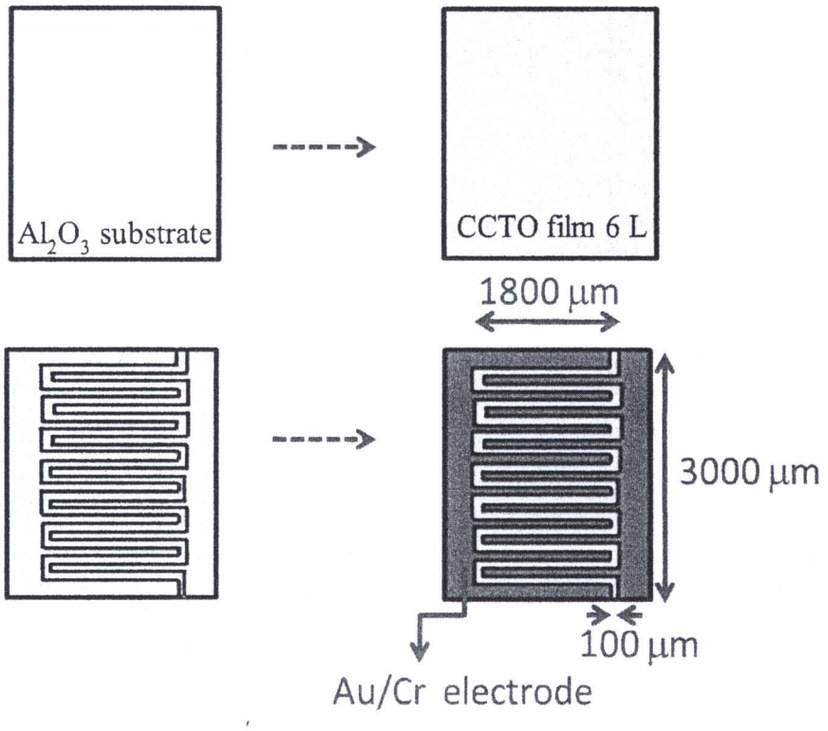

Figure 5.23: CCTO thin films with interdigitated electrode.

Figure 5.24 shows (a) the capacitance (b) dielectric constant and (c) loss tangent of the CCTO films before gamma radiation. Figure 5.25 shows (a) the capacitance (b) dielectric constant and (c) loss tangent of the CCTO films after gamma radiation dose of 5 kGy. respectively. From Fig. 5.24(a) and Fig. 5.25(a), the capacitance of the film before gamma ray irradiation which increases from 1.36 - 1.22 pF to 1.62 - 1.36 pF in 10 kHz - 1 MHz frequency range after gamma ray irradiation with 5 kGy doses. Our results increasing of capacitance values are consistant with other works [13]. Arshak et al. [13] found that the capacitance for ZnO thick film exhibited from 21.58 pF at a dose of 1 mGy to 28.33 pF at 2.3 mGy dose and thick films of SnO_2 also showed an increase in the capacitance from 5.05 pF before irradiation to 8.69 pF at a dose 0.46 mGy. However, our CCTO film based on the change of capacitance is not that sensitive to gamma rays like as ZnO and SnO_2. From Fig. 5.24(b) and (c) and Fig. 5.25(b) and (c), the dielectric constant of the CCTO film increasing from 314 - 280 to 552 - 308 and loss tangent of CCTO film increasing from 0.020 - 0.013 to 0.138 - 0.030. The observed increase in dielectric constant values with increasing dose may be attributed to a gradual formation of mobile charge carriers or easily orientable dipolar molecules that are capable of conducting the electric current. These charge carriers or dipolar molecules could be formed from structural modifications caused by gamma ray irradiation [55, 56, 57].

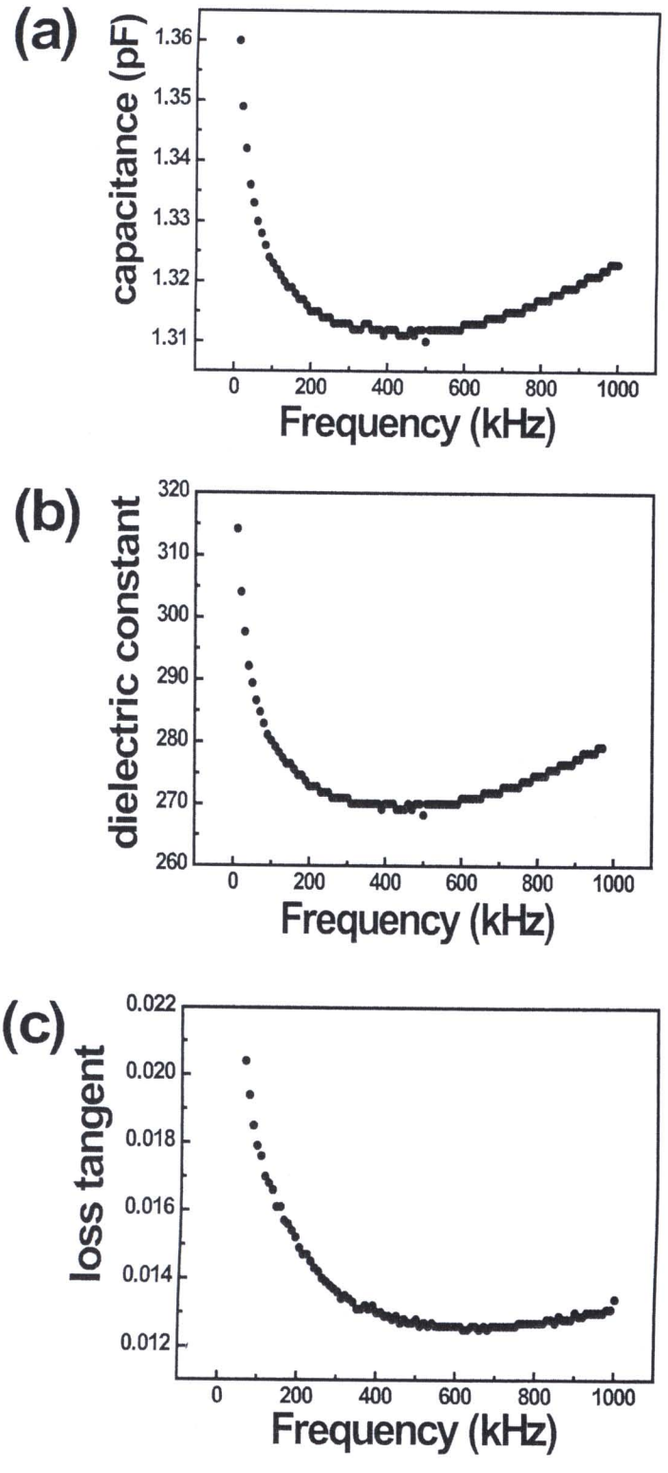

Figure 5.24: The (a) capacitance (b) dielectric constant and (C) loss tangent of CCTO films before gamma radiation.

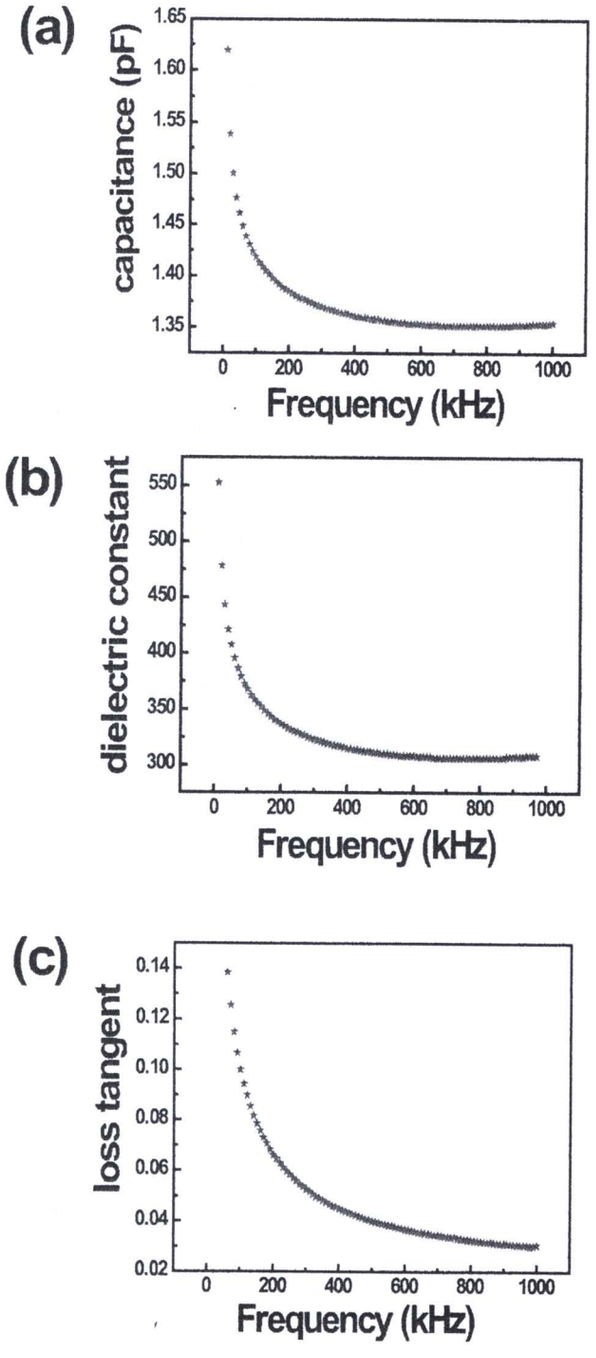

Figure 5.25: The (a) capacitance (b) dielectric constant and (C) loss tangent of CCTO films after gamma radiation dose of 5 kGy.